

Natural patterns and wavelets

C. Bowman and A. C. Newell

Mathematics Institute, University of Warwick, Coventry CV4 7AL, United Kingdom

An introductory review of pattern formation in extended dissipative systems is presented. Examples from many areas of physics are introduced, and the mathematical analysis of the patterns formed by these systems is outlined, for patterns near and far from onset. The wavelet transform is introduced as a useful tool for the extraction of order parameters from patterns. [S0034-6861(98)00401-2]

CONTENTS

I. Introduction	289
II. Observations	289
III. Why Do Patterns Appear?	292
IV. Mathematical Analysis Near Onset	294
A. Determination of a local planform	295
B. Slow modulation of patterns of rolls near onset	296
V. Analysis Far From Onset	297
VI. Wavelets—A Bridge Between Theory and Experiment	299
VII. Conclusion	300
References	300

I. INTRODUCTION

Natural patterns turn up all over. They show up as ripples in the sand washed by the tide or blown by a dry desert wind. One sees them on the tips of one's fingers as fingerprints, as well as in the stripes of a tiger or zebra and the spots of a leopard (see Murray, 1989). Patterns occur in galaxies and stars, in the atmosphere and in the oceans, in geological formations, and in plant morphology. They turn up in the laboratory as well, in experiments designed to measure the heat transfer of convecting fluids, the strengths of thin shells, the behavior of wide-aperture ("fat") lasers, or the nature of flame fronts. This is a colloquium about the reasons for the appearance of such similar structures in physically diverse systems and about the attempts to integrate the spectrum of pattern behavior into a mathematical framework that will display the underlying mechanisms behind the spontaneous formation of patterns.

The notion of pattern formation does not attach itself exclusively to any particular area of science. Rather it cuts across disciplines; the patterns seen in convecting fluids have much in common with those seen in lasers, on buckling shells, in interacting chemicals, etc. The central theme in the study of patterns, therefore, is to understand the rules determining the large-scale (macroscopic) behavior of patterns which may arise from a large class of physical (microscopic) systems. The fact that virtually the same patterns occur in widely different physical contexts suggests that one should look for their common symmetries, for general principles that underlie their formation, and for descriptions that emphasize

their macroscopic structure. Connected with this task is the effort to find a tool for mapping the connections between data provided from experimental (see Assenheimer and Steinberg, 1994) and computed patterns (Pesch, 1996) and those macroscopic order parameters which arise naturally from the theoretical approaches. There is just such a tool available. It is called the continuous wavelet transform.

The aims of this essay are to convey the message that patterns and their defects are macroscopic objects with universal behaviors and to communicate some of the excitement and importance of the field. Open any journal these days in physics, chemistry, biology, ecology, or the mathematical sciences, and you will find several articles on pattern formation. One of the reasons for this interest is a curiosity as to why complicated systems organize themselves into ordered structures. Another is that more powerful methods (experimental, computational, and analytical) are becoming available to help us understand pattern behavior. There is also the possibility of technological payoffs from understanding patterns. Can they be used to store information in an efficient way? Can we learn to control the instabilities in the patterns, so as to construct more powerful laser arrays, or to maximize heat transport in fluids? But perhaps the purest reason of all to study patterns is the simplest. Like all beautiful things, they are an interplay of order and disorder, mysterious and intriguing and full of open challenges for the fertile imagination to explore.

II. OBSERVATIONS

Before launching into the mathematical description of patterns, it is reasonable to consider some examples of the kinds of patterns that occur both in nature and in the laboratory. Figures 1–15 show examples of patterns that are observed experimentally or that arise in numerical simulations. They fall into several classes.

First, Figs. 1 and 2 show a pattern of oriented stripes in sand and on the surface of an angelfish, the *Pomacanthus Imperator*. The former arise as a consequence of wind/sand interaction. The deformation of the sand consists of almost straight parallel stripes across (normal to) the direction of the wind. Nonuniformity in the local wind strength produces nonuniform wavelengths in the



FIG. 1. Sand waves on the Arizona desert.

sand waves. In all probability, the latter arise as the result of a diffusively driven instability in a reaction-diffusion system. In both the sand and the fish, there is nonuniformity in the pattern, either as a result of varying wind strength or due to the shape of the fish. As a consequence of this nonuniformity, point defects called dislocations are formed (where two wave crests merge into one). Defects will play an important part in the story of patterns. They too exhibit certain universal features.

The second class of patterns in Figs. 3, 4, and 5 comes from both experimental and numerical simulation of convection in fluids, and from domains in ferrimagnetic garnet films. Despite the fact that, at a microscopic level, the ferrimagnetic system has little in common with fluid convection, it displays the same sort of pattern. This emphasizes one of our central points, that similar patterns occur in what are physically very different systems. In the convection experiment, fluid in a thin container is heated from below and begins to convect, with the hot fluid rising to the top of the cell. In these experiments, the motion of the fluid takes the form of a horizontal rolling cylinder, with hot fluid rising on one side while cooler fluid descends on the other. The bright and dark lines in the picture are the loci of minimum and maxi-

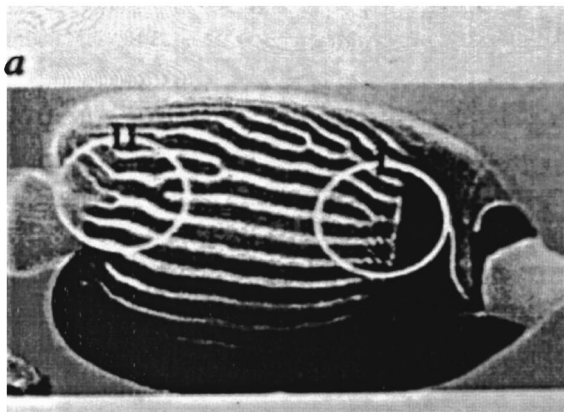


FIG. 2. Stripe pattern of *Pomacanthus Imperator* (Kondu and Asai, 1995).



FIG. 3. Pattern from experimental Rayleigh-Bénard convection (Surko, 1993).

um temperatures, respectively. They are produced by shining light through the convecting layer of fluid. The refractive index of the warmer, rising fluid is lower than that of the colder, descending fluid, and consequently the light focuses on the contours where the temperature is lowest, creating the visual contrast. The local planforms (tilings of the plane) in these patterns are again stripes (or rolls), but the directional preference has been removed, and the choice of local direction is made by a local bias. Consequently the pattern consists of a mosaic of striped patches with similar wavelengths but unrelated directions. Inside an individual patch both the wavelength and the direction of the rolls are nearly constant. Neighboring patches are mediated by line defects called phase grain boundaries and amplitude grain boundaries (PGBs and AGBs, respectively) which themselves meet at point defects. At PGBs the rolls bend sharply, but no new rolls are formed, while AGBs look like chains of dislocations.

Mathematically, it is convenient to think of a patch of rolls as a 2π periodic function,

$$f\left(\theta = \int \mathbf{k} \cdot d\mathbf{x}; A\right), \quad (1)$$

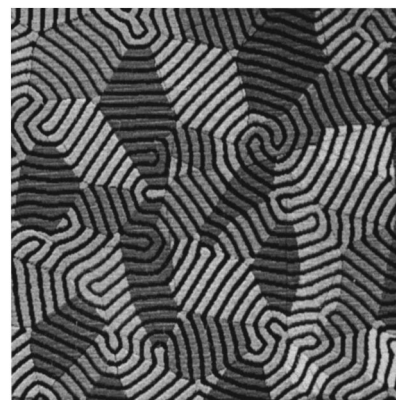


FIG. 4. Magnetic domains in a ferrimagnetic garnet film with roll patches shaded according to their orientation (Seul *et al.*, 1991).

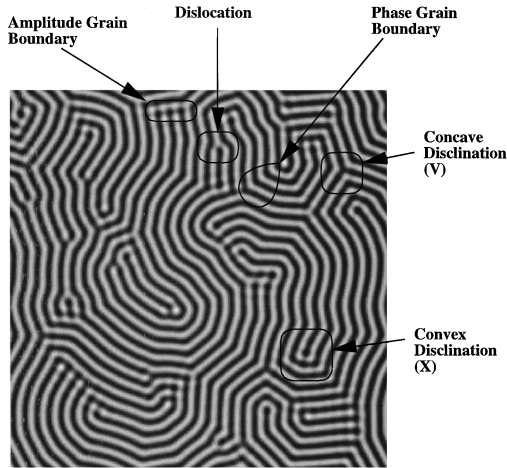


FIG. 5. Numerical simulation of Rayleigh-Bénard convection at infinite Prandtl number. Various forms of pattern defects are marked.

of a phase θ whose local gradient $\nabla\theta = \mathbf{k}$ gives the local direction normal to the roll axes and the local wavelength $\lambda = 2\pi/k$, where $k = |\mathbf{k}|$. The parameter A measures the local amplitude of the pattern. Notice that in all the examples A and \mathbf{k} change much more slowly than the microscopic field f everywhere in the pattern except at line and point defects. PGBs are places where the phase is continuous, but the pattern wave vector changes abruptly, while AGBs are discontinuities in the phase of the pattern and zeros of the amplitude. PGBs meet and terminate at several types of point defects, the most important of which are called concave and convex disclinations, which we shall denote as V and X, respectively (V for concaVe, X for conveX). These objects are very important, as all point defects of two-dimensional patterns turn out to be composites of V and X. Examples of these defects are shown in Figs. 5 and 18.

The third class of patterns, shown in Figs. 6 and 7, again comes from experiments with fluid convection, but at different parameter values, at which the dominant planforms are targets and spirals. One striking difference between Fig. 3 and Fig. 6 is the absence of PGBs and disclinations. In general, sharp corners seem to have

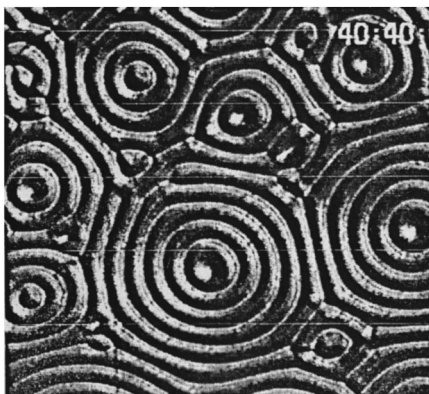


FIG. 6. Target pattern in experimental convection with low Prandtl number (Assenheimer and Steinberg, 1994).

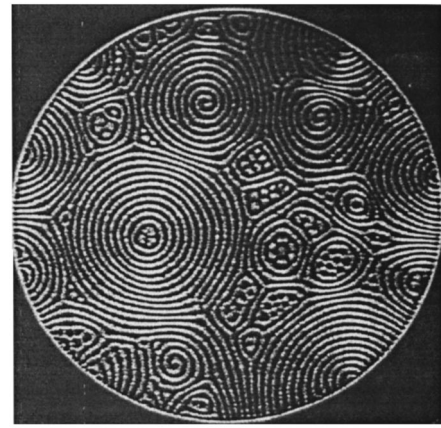


FIG. 7. Target pattern in experimental convection. Hexagons appear at point defects and target cores (Assenheimer and Steinberg, 1996).

been replaced by rounder ones, although again a particular wavelength is dominant. One reason for this is the presence of a soft mode in the system (in this case, the vertically averaged flow of fluid in the horizontal plane). Horizontal pressure differences induced by the spatially nonuniform pattern drive these slow horizontal currents, which in turn serve to advect the phase contours of the pattern. This horizontal flow serves to round off sharp PGBs. Soft modes like this are not only present in fluid systems; they are ubiquitous and arise as a consequence of some overall symmetries rather than the system details. Many features of this class of patterns are still not understood: the emergence of targets, the transitions to spirals, the coexistence of hexagonal and roll (in target form) planforms.

In the fourth class of patterns, shown in Figs. 8–11, a different planform, the hexagon, is dominant. Indeed, in extended, two-dimensional patterns with rotational symmetry, and near the initial onset of the pattern, hexagons are the generic planform. Only the presence of another symmetry inhibits them. The hexagon is (approximately)

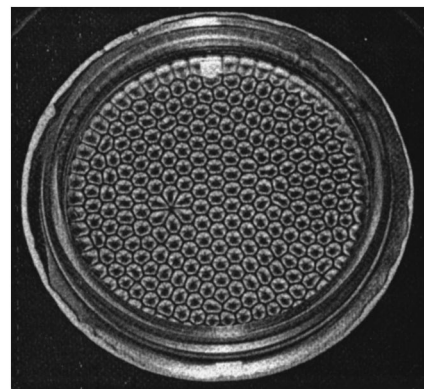


FIG. 8. Imperfections in a hexagonal Bénard convection cell. Aluminum powder shows the motion of a thin layer of silicone oil on a uniformly heated copper plate. The deformity to the left of the pattern is caused by a tiny dent in the plate (Koschmeider, 1974).

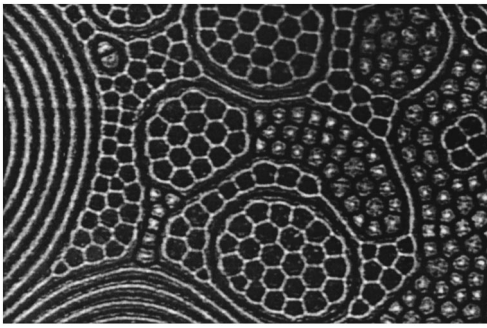


FIG. 9. Convection pattern showing, besides rolls, patches of up and down flow hexagons (Assenheimer and Steinberg, 1996).

a superposition of three roll configurations, and the penta-hepta defect seen in Fig. 11 is simply a dislocation in one of the roll fields. You can see this by running your eye along the figure in a vertical direction. Figure 12 shows yet another planform, the square. This figure comes from convection in liquid crystals.

In Fig. 13, taken from a numerical simulation of a Raman laser, and Fig. 14, from experimental convection in binary fluids (both He^3/He^4 and water/alcohol mixtures will do), the dominant planform is again the roll, but this time the roll crests travel the direction of their wave vector. These configurations tend to exhibit behavior typical of dispersive wave packets. Like wave packets, they bunch up into regions of high and low amplitudes.

Finally, in Fig. 15, we show an example, taken from an experiment on Faraday waves, of an exotic cocktail of pattern structures, far richer than rolls, hexagons, or squares. In this case, the planform is the superposition of six roll patterns, equally spaced around the circle (compared to the three roll modes present in the hexagonal planforms), resulting in a planform of 12-sided polygons. Since 12-sided polygons cannot tile the plane, they are each surrounded by 12 pentagons to fill space.

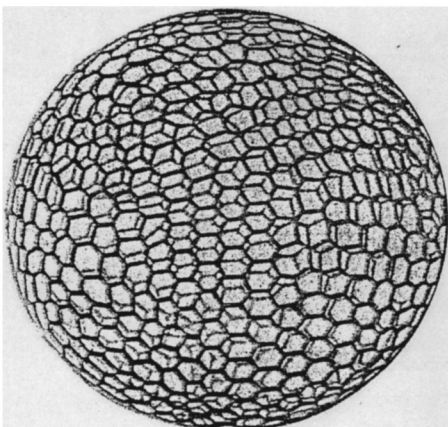


FIG. 10. Skeleton of the Radiolonia Aulonia Hexagona (Thompson, 1942).

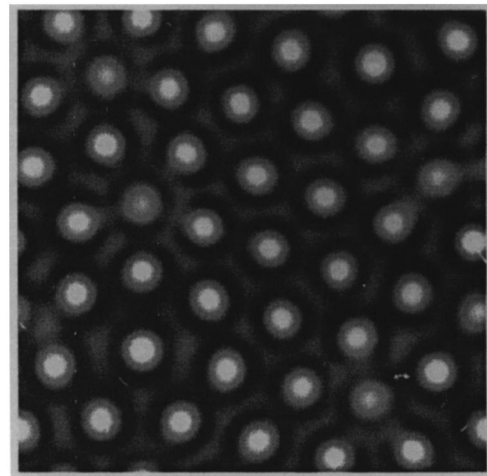


FIG. 11. Near-field, stationary light intensity pattern on two counter propagating laser beams at subcritical values of beam intensity in a weakly nonlinear Kerr focusing medium. The basic pattern is hexagonal. Observe the presence of a penta-hepta defect (bright spots surrounded by five or seven neighbors).

III. WHY DO PATTERNS APPEAR?

The patterns we talk about in this article arise in systems that are dissipative and driven far from equilibrium by some external stress (see Cross and Hohenberg, 1993). Spatially extended means that the spatial size of the system in at least one direction, l , is much larger than the pattern wavelength λ . The ratio $1/\epsilon = l/\lambda$ is called the aspect ratio of the system, and it is large. The dissipative nature of the system means that, for small values of the external stress parameter, the spatially and temporally uniform state of the system is (usually) stable. However, as the stress is increased, the uniform state can become unstable to perturbations of a certain wavelength, which reflects some length scale in the microscopic system. Generally speaking, this wavelength allows the system to change in response to the stress, while overcoming dissipation. At this critical value of

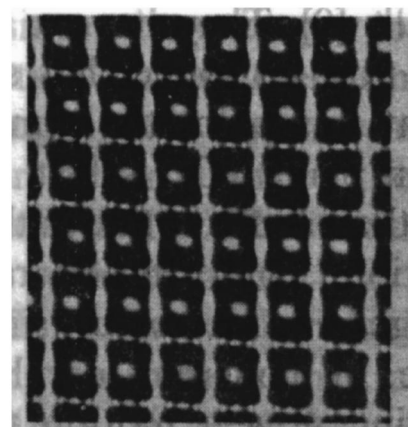


FIG. 12. Square pattern from convection in liquid crystals (Jots and Ribotta, 1986).

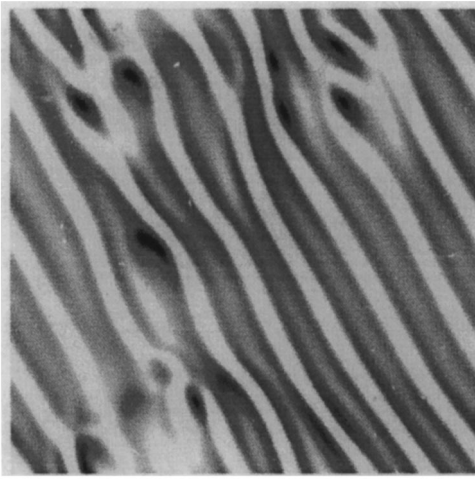


FIG. 13. Supercritical traveling-wave state of a Raman three-level laser.

the stress parameter, the state of the system changes abruptly and qualitatively (a phase transition). Certain shapes and configurations are preferentially amplified and grow to new equilibrium values. This leads to the appearance of self-organization and order, resulting in what we have been calling a pattern. At these phase transitions, or bifurcations, some, although not all, of the symmetries of the original state are destroyed, and the system is attracted to a new solution, such as, for example, the roll pattern in Fig. 5. As the stress continues to increase, this new solution can itself become unstable, leading to more symmetry breaking and more complicated states, which can be time dependent, chaotic, and eventually quite turbulent (see Gollub and Swinney, 1975).

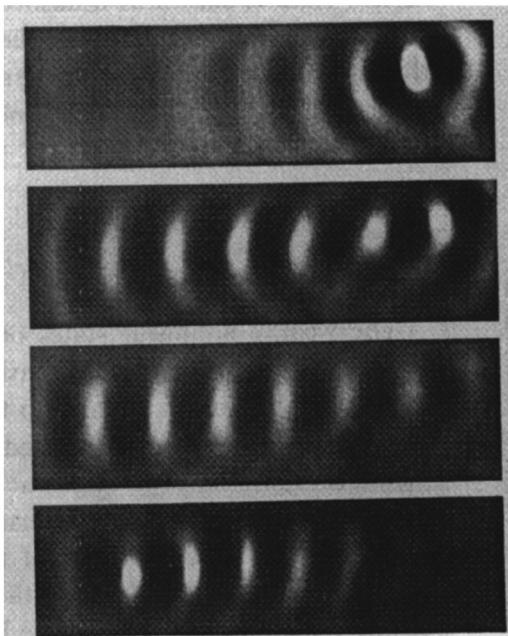


FIG. 14. Shadowgraph images taken of convection in binary fluid mixture (Kolodner *et al.*, 1989).

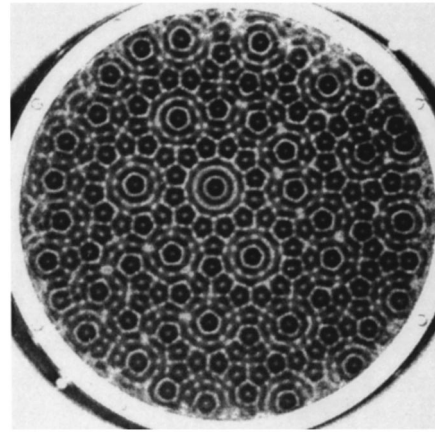


FIG. 15. Quasicrystal pattern from the vertical oscillation of a container filled with fluid (the Faraday experiment) with two simultaneous forcing frequencies (Edwards and Fauve, 1994).

The granddaddy of all pattern-forming systems is convection in a thin, horizontal layer of fluid, often associated with the names Rayleigh and Bénard (Rayleigh, 1916; Bénard, 1990). It is a very rich system and provides a useful paradigm for pattern formation in general. In addition it is an easy system to visualize, and most of the intuition and knowledge that is needed to understand what is going on involves high school physics and undergraduate mathematics. Consider a thin horizontal layer of fluid between two plates, extended for a long distance transversely, as shown in Fig. 16. Heat this system from below by setting the bottom plate to a temperature ΔT °C hotter than the top. The hot fluid at the bottom of the cell, now less dense because of thermal expansion, becomes buoyant and wants to move upwards. If ΔT is small enough, the fluid viscosity will counteract this upward force, and the heat will simply conduct through the fluid from bottom to top. But if we raise ΔT above some

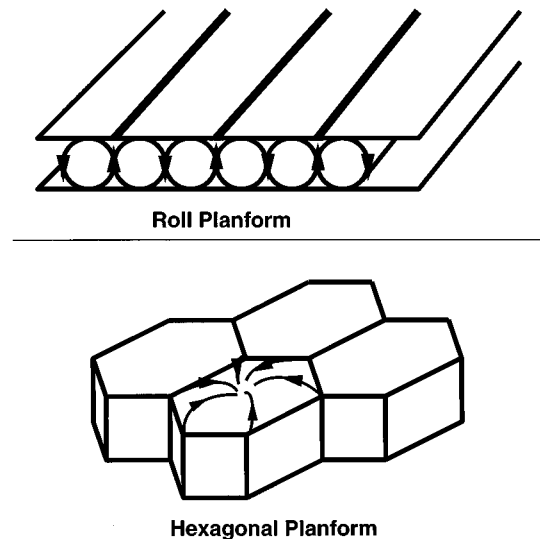


FIG. 16. Schematic diagram of Rayleigh-Bénard convection, showing (a) rolls and (b) hexagons, with downward fluid motion at the hexagon center.

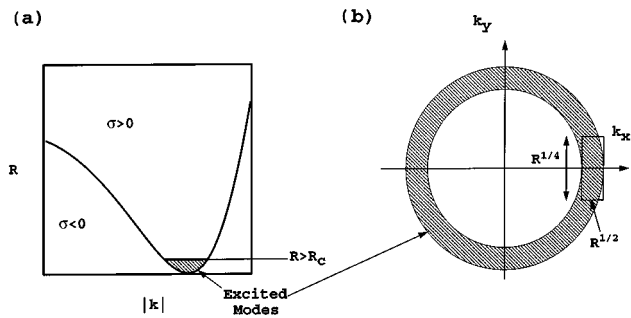


FIG. 17. Linear stability analysis for Swift-Hohenberg equation: (a) neutral stability curve ($\sigma=0$); (b) excited modes in two dimensions. The box shows the modes around $\mathbf{k}=(1,0)$ which are accounted for in Eq. (6).

critical value, this mode of heat transport will not be efficient enough to handle the increased load. The viscosity will no longer counteract the buoyancy, and the hot fluid will rise to the top. The hot fluid cannot rise everywhere uniformly, however, since the cold fluid must move down somewhere! Thus the initiation of convection breaks the translational symmetry of the pattern in the horizontal direction. This symmetry breaking is shown in Fig. 16, in the guise of both convection rolls and hexagons. In the former the fluid flows in circles on a horizontal cylinder, whose width is equal to the wavelength of the roll pattern, with the hot fluid rising on one side of the cylinder, cooling at the top plate, and then

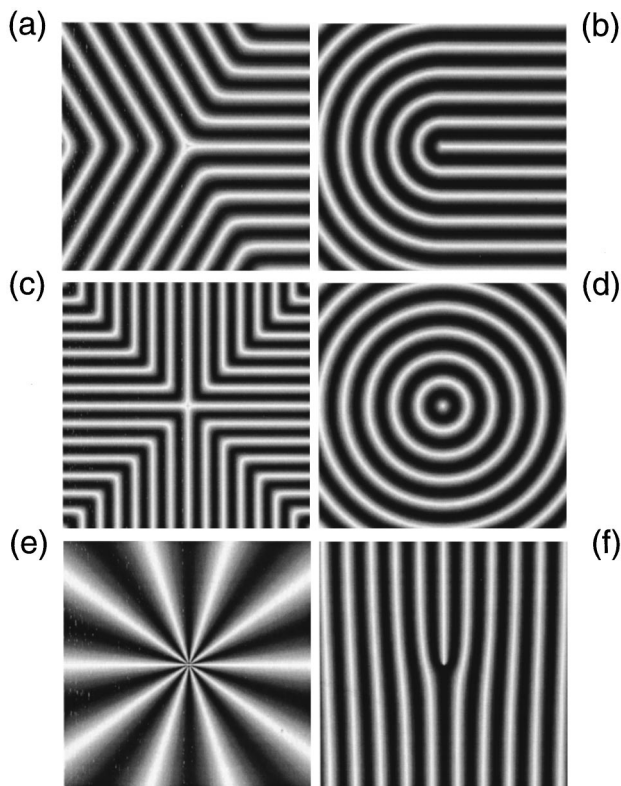


FIG. 18. Assorted pattern defects: (a) concave disclination, (b) convex disclination, (c) saddle, (d) target, (e) vortex, and (f) dislocation.

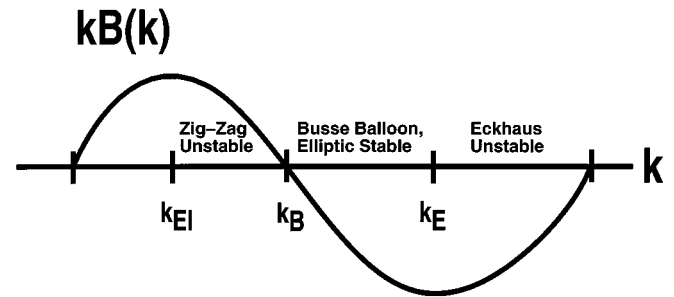


FIG. 19. Typical form of the phase diffusion function $B(k)$, with stability boundaries marked.

falling back to the bottom again. It is easy to see that this cylinder will have a preferred width, which in turn leads to a preferred wavelength in the pattern. If the rolls are too fat, the viscous dissipation on the top and bottom plates is excessive; if the rolls are too thin, the rising and falling fluids are in close contact with each other, and “dissipation” comes from both thermal conductivity effects [there is heat transfer between the rising (hot) and the descending (cold) parcels of fluid, which reduces the buoyancy of the former], as well as viscous stress between the rising and falling fluid. The optimal cylinder width gives rise to a pattern with wavelength λ of the order of d , the container thickness.

In hexagonal configurations, the warm parcels can rise (or descend) like plumes along the core of an apple, and then descend (or rise) along the apple’s surface. The air motion that leads to the formation of cumulus clouds is a good example of this type of convection. Observe that there is a fundamental difference between the roll and hexagon states. In the former, there is no preferred up/down direction, and an upflow can be turned into a downflow by a translation of $\lambda/2$. On the other hand, with the hexagons there is no translation that will reverse flows in the center of the hexagon from upward-moving to downward-moving. Because of this, rolls will dominate if the problem has a strong symmetry about the horizontal midplane.

IV. MATHEMATICAL ANALYSIS NEAR ONSET

Let us consider the convection problem again, this time with a little mathematics thrown in. Consider, as a model for pattern formation, the “Swift-Hohenberg equation” (Swift and Hohenberg, 1977)

$$\frac{\partial w}{\partial t} + (\nabla^2 + 1)^2 w - R w = -w^3, \quad (2)$$

where w represents the vertical fluid velocity (see Cross and Hohenberg, 1993). This is perhaps the simplest non-trivial model imaginable for the fluid convection problem. It is obtained by applying some fairly brutal approximations to the real fluid equations, but nevertheless it contains some of the same symmetries and its solutions exhibit the same qualitative features found in real fluids. It is an excellent toy model on which to develop insight and intuition. The $w=0$ solution cor-

responds to the conduction solution in the fluid convection problem. The first goal of analysis is to find the critical value R_c of the stress parameter R at which the conduction solution loses its stability and identify the set of shapes that play an important role when $R - R_c$ is positive and small. This is accomplished through linear stability analysis. Linearize the equations around $w=0$ by letting $w=0 + \delta w$ and ignoring quadratic and higher powers of δw . Now write δw in terms of its Fourier series, $\delta w = \hat{w}(t) \exp(i\mathbf{k} \cdot \mathbf{x})$, and obtain $\hat{w}(t) = \hat{w}(0) \exp(\sigma(R, k)t)$, with $\sigma = R - (k^2 - 1)^2$.

Since we are interested in the value of R where the uniform solution first loses its stability, we look for the minimum value of R (with respect to k) on the neutral stability curve $\sigma=0$ (see Fig. 17). This happens for $R = R_c = 0$, and $k = k_c = 1$. At $R=0$, all modes $e^{i\mathbf{k} \cdot \mathbf{x}}$ with $k = |\mathbf{k}| = 1$, or any linear combination thereof, lose stability and become candidates to replace the conduction solution $w=0$. When R increases to a value above zero, nonlinear terms [in Eq. (2), the w^3 term] come into play and various configurations consisting of linear combinations,

$$w(\mathbf{x}, t) = \sum_1^N [A_j(t) \exp(i\mathbf{k}_j \cdot \mathbf{x}) + (*)], \quad (3)$$

[where (*) denotes complex conjugate, so that w is real], compete for dominance. The winning configuration is the planform that is observed. Sometimes there can be more than one winning configuration, in which case the initial conditions determine which state is realized. Configurations with $N=1$ correspond to rolls; those with $N=3$ and $\mathbf{k}_1, \mathbf{k}_2$, and \mathbf{k}_3 120° apart in direction correspond to hexagons. We shall return to this competition in more detail shortly, after taking a closer look at the degeneracies and near degeneracies of the linear stability problem.

Degeneracy in this context refers to the fact that there is not one unique mode excited as $R \rightarrow R_c$. There are several sources of degeneracy in this problem. The first arises as a consequence of the rotational symmetry enjoyed by the conduction solution and manifests itself in the fact that all modes \mathbf{k} with $k=1$ have the same growth rate. A second source of degeneracy arises from the fact that, for $R > 0$, the set of excited modes is not a circle at $k=1$, but rather an annulus, with width $2\sqrt{R}$, around the circle $k=1$. All the modes in this annulus will in principle be candidates in the competition for dominance once $R > 0$. But there are other players in the game which also must be considered. They too arise from symmetries and correspond to Fourier modes that are neither excited nor damped for any value of R . These modes can thus be generated easily by nonlinear interactions with the amplified modes once the pattern begins to emerge. Such modes are generally referred to as soft, or Goldstone, modes of the system. In Eq. (2) there are no such modes, but in the real fluid convection problem the horizontal mean flow is an example of such a soft mode when the viscosity is small; it corresponds to the horizontal Galilean symmetry of the system in the inviscid limit.

Life would have been easier (and less interesting) if the linear stability theory had shown that of all the possible configurations of the system \mathcal{S} , only a finite number of modes were excited and the rest were strongly damped. Call the set of excited modes \mathcal{A} for active and the rest of the modes \mathcal{P} for passive. The amplitudes of the active modes are called the order parameters. When $R - R_c$ is small and positive, the amplitudes of all the modes in \mathcal{P} rapidly decay. Thus their initial values can be ignored, and we have only to worry about their being regenerated by the nonlinear interactions of members of \mathcal{A} . But then the amplitudes of the regenerated passive modes are simply determined algebraically by the order parameters. A graph of the amplitude of the passive modes as a function of the amplitudes of the active modes, written $\mathcal{P} = \mathcal{P}(\mathcal{A})$, is called the center manifold M of the system at R . For $R - R_c$ small, an initial point in the phase space of the system is attracted quickly to M and, on M , a slow dynamics (the time scale is the inverse of the growth rate) involving a competition between the order parameters takes place.

In our case, however, because of the degeneracies, there is no clean and unambiguous separation of modes into \mathcal{A} and \mathcal{P} . The continuum of modes on $k=1$ all grow at the same rate, and the modes in the surrounding annulus of width $2\sqrt{R}$ exhibit a continuous set of growth rates from R to 0. Even the modes outside but close to this annulus do not decay sufficiently fast that we can lump them together into \mathcal{P} . Indeed, the general problem is still open. We simply do not have a convenient mathematical description for functions whose Fourier transform has its support in an annulus around some curve. So we do the best we can by arguing (i) that, very close to $R=0$, the local planform is chosen by the competition between a finite number of modes lying on $k=1$ because they grow the fastest, and once established, inhibit the rest, and (ii) once the local planform is selected, the modes in the neighborhood of the active modes serve only to modulate this local planform slowly, over long distances. The reader can find the details of this analysis in Cross and Hohenberg (1993; see also Joseph, 1976; Newell, Passot, and Lega, 1993; and Pesch, 1996). Here we sketch the results in narrative form.

A. Determination of a local planform

For $R > R_c$ and small, expand $w(\mathbf{x}, t)$ in powers of amplitude

$$w = \sum_1^N [A_j(t) \exp(i\mathbf{k}_j \cdot \mathbf{x}) + (*)] + \text{corrections}, \quad (4)$$

with $|\mathbf{k}_j| = 1$, $j = 1 \dots N$, and substitute into the microscopic field equation, Eq. (2). One finds that the correction terms can only be solved for if the growth rate of each A_j is given in a power series in powers of $\{A_l\}_{l=1}^N$. For Eq. (2) this solvability condition is

$$\frac{\partial A_j}{\partial t} = R A_j - 3 A_j^2 A_j^* - 6 A_j \sum_{l \neq j} |A_l|^2. \quad (5)$$

More generally, however, the microscopic equation will contain quadratic nonlinearities, and these will lead to

an additional term involving the quadratic product of those amplitudes A_p , and A_q , such that the sum of their wave vectors resonates with $-\mathbf{k}_j$, namely, $\mathbf{k}_p + \mathbf{k}_q = -\mathbf{k}_j$, with $|\mathbf{k}_p| = |\mathbf{k}_q| = |\mathbf{k}_j| = 1$. This can happen only for wave vectors 120° apart. Thus the appearance of this additional term, which is proportional to $A_p^* A_q^*$ in the above Landau equation (5) leads to the possibility that the hexagonal planform is dominant. In fluid convection, the coefficient of this term is zero, leading to the dominance of rolls, when there is symmetry about the midplane of the convection layer. But if that symmetry is broken, say by a temperature-dependent viscosity, then the hexagonal planform will be seen near onset. Furthermore, it can appear as a subcritical bifurcation, namely at values of $R < R_c$. So the local planform is chosen by looking for the stable equilibrium of Landau equations, such as Eq. (5). In most cases, this can be accomplished by minimizing a *free-energy functional* containing quadratic, cubic, and quartic products of order parameters. For the multimode configuration to dominate over the single one is rare (except when the quadratic terms are important) and only happens when the coupling coefficient β_{jl} in the cubic terms in Eq. (5) ($\beta_{jl} = 6$ in our example) has special properties. A good challenge for the reader is to characterize the properties of β_{jl} for $N = 2, 3, 6$ and $n \gg 1$ mode configurations to give the lowest free energy (see Newell, Passot, and Lega, 1993).

B. Slow modulation of patterns of rolls near onset

For now let us suppose the modal analysis discussed above allows one to conclude that we have a pattern with a roll planform. This analysis only settles the question of local planform. It tells us nothing about the situations in Figs. 3 and 4, where rolls of one orientation impinge on a neighboring patch of rolls of a different orientation. It says nothing about the slow bending of rolls, nothing about the labyrinthine patterns of Fig. 5, and nothing about the targets and spirals of Fig. 6. Neither would it describe the hepta-penta dislocations seen in the hexagonal lattice of Fig. 11, nor the change in orientation of hexagons from one place to another.

These spatial variations have their origins in the two degeneracies evident in Fig. 17. Because of the rotational degeneracy, it will be local biases, often but not always due to the boundary conditions, which determine the local roll orientation. Thus roll patches with different orientations will emerge at different places in the pattern and need to be connected to each other via line and point defects. Furthermore, because of the bandwidth degeneracy, there is a certain narrow band of wavelengths which can be tolerated by the system. Thus the wavelength of the pattern can change slowly from one place to another.

How can one describe such behavior analytically? Unfortunately, as we have said, there is no convenient mathematical description of functions whose support is confined to an annular region of a curve in Fourier space. Indeed, this is an open problem on which new ideas are needed. Nevertheless, there are some avenues

open. First one can ask for a description that incorporates a finite bandwidth of modes about a fixed wave vector, say $\mathbf{k} = (1, 0)$. Such descriptions are possible by approximating the annular region near $(1, 0)$ by a rectangle (see Fig. 17) with width equal to $R^{1/2}$ and a height of $R^{1/4}$. With this consideration, the amplitude of the pattern $W(T = Rt)$ becomes instead an *envelope*, a function $W(X = R^{1/2}x, Y = R^{1/4}y, T = Rt)$ that depends slowly on the space and time coordinates. With this added flexibility, new terms involving the spatial derivatives of W appear in the evolution equation (5), which becomes, for $N = 1$ and $\mathbf{k} = (1, 0)$, the Newell-Whitehead-Segal (NWS) equation,

$$\frac{\partial W}{\partial T} - 4 \left(\frac{\partial}{\partial X} - \frac{i}{2} \frac{\partial^2}{\partial Y^2} \right)^2 W = RW - 3W^2W^*. \quad (6)$$

Equation (6), which is universal, describes many of the important features of patterns. If the rolls are traveling rather than stationary, the coefficients become complex, so as to incorporate nonlinear and dispersive wave effects, leading to what is known as the class of complex Ginsberg-Landau equations (see Newell, Passot, and Lega, 1993) or complex Swift-Hohenberg equations (see Lega *et al.*, 1995). Such a description allows one to test the stability of sideband solutions,

$$W = \sqrt{\frac{1 - 4K^2}{3}} \exp(i\mathbf{K} \cdot \mathbf{X}). \quad (7)$$

These solutions of the amplitude equations correspond to roll solutions of the original equations [Eq. (2)] with wave number $1 + \sqrt{R}K$. The region of existence of these solutions is given by $K^2 < 1/4$, which corresponds to $(k - 1)^2 < R$, the parabola that fits the neutral stability curve of Fig. 17 at $k = 1$. The region of stability of these solutions, however, is smaller, given by $0 \leq K \leq 1/2\sqrt{3}$. For wave numbers k that correspond to $K > 1/2\sqrt{3}$, the mode $(k, 0)$ undergoes what is known as an Eckhaus instability to reduce its wave number. In two dimensions this instability is not saturated and leads to the creation of a pair of dislocations which move apart along roll lines, removing a roll from the pattern. This is exactly what is happening on the skin of the *Pomacanthus Imperator* in Fig. 2.

For patterns with wave number $k < 1$ ($K < 0$), the mode with wave number $(k, 0)$ gives up its energy to conjugate modes with wave number $\mathbf{k}_\pm = (k, \pm \sqrt{1 - k^2})$ via a nonlinear four-mode interaction, $2\mathbf{k} = \mathbf{k}_+ + \mathbf{k}_-$. This instability is saturated by a zigzag pattern with alternating patches of wave numbers \mathbf{k}_+ , and \mathbf{k}_- . Equation (6) admits solutions which correspond to the transition between zig and zag regions. These solutions correspond to (weakly bent) phase grain boundaries. We challenge the reader to verify that

$$W = A(\phi_X, \phi_Y) \exp[i\phi(X, Y)] \quad (8)$$

with $\phi = -KX + \ln 2 \cosh \sqrt{2K}Y$ and $k = 1 - \sqrt{R}K$, is a solution of Eq. (6) describing the evolution from a zig state [$W \approx (\sqrt{R}/3) \exp(ikx - i\sqrt{2K}\sqrt{R}y) + (*)$] as $Y \rightarrow -\infty$]

to a zag state [$W \approx (\sqrt{R/3}) \exp(ikx + i\sqrt{2K\sqrt{R}}y) + (*)$ as $Y \rightarrow \infty$]. Find A as a function of ϕ_X and ϕ_Y , and verify that it tends to $\sqrt{R/3}$ as $Y \rightarrow \pm\infty$.

V. ANALYSIS FAR FROM ONSET

In the previous subsection, we introduced the concept of the envelope order parameter to capture the behavior of patterns that everywhere in space had their wave numbers \mathbf{k} close to $(1,0)$. This analysis assumed, however, that R was close to R_c and the amplitude of the new state was small. When dealing with patterns far from onset, this small parameter is no longer available, and another approach is necessary. To find this new approach, we need to go back to the patterns themselves. Look at Figs. 1–7 and suppose someone were to ask you to suggest one piece of information at each point which best describes the pattern macroscopically, i.e., a quantity that changes slowly (significant changes occur only over many pattern wavelengths) almost everywhere. One natural choice is the pattern wave vector \mathbf{k} , the gradient of the local phase of the pattern. This vector field is normal to the rolls of the pattern everywhere and has a magnitude proportional to the inverse of the pattern wavelength. The wave vector characterizes the pattern, since the microscopic field can be reproduced from the wave vector information (modulo an amplitude factor) by simply writing it as a periodic function of the phase $\theta = \int \mathbf{k} \cdot d\mathbf{x}$. Away from defects, \mathbf{k} changes slowly compared to the pattern wavelength, making it a truly macroscopic quantity, so the choice is a good one. The wave vector \mathbf{k} is indeed the most important macroscopic coordinate, or order parameter, of the pattern. In the near-onset situation, \mathbf{k} is simply the unit vector in the x direction plus the imaginary part of $(W^*)^{-1} \nabla W$.

The astute reader may note that there is a problem in producing the phase θ for several reasons. First of all, if the pattern contains dislocations or other amplitude defects, the wave vector field \mathbf{k} need not be curl free, making the phase ill defined. This is not a terribly important difficulty, since we are concerned not with the phase of the pattern, but rather with a 2π -periodic function of that phase, and this periodicity will wash out the multivaluedness introduced by the nongradient part of \mathbf{k} . Another, perhaps more fundamental problem in the definition of θ is the fact that \mathbf{k} is not actually a vector field at all. There is no way in principle to distinguish rolls with wave vector \mathbf{k} from rolls with wave vector $-\mathbf{k}$. This may seem to be an unimportant detail, but in fact it is of fundamental importance in the lives of some defects.

Look at any disclination shown in Figs. 3–5 which have been redrawn alone in Figs. 18(a), 18(b). Now pick any closed curve around the center of either disclination and continuously follow the wave vector around it. Notice that the wave vector changes sign as this curve is circumscribed. These disclinations cannot exist as point singularities of ordinary vector fields. To include them in our description, we have to consider \mathbf{k} as a director field (a vector field without the arrowheads). It is perfectly

fine to think of \mathbf{k} as a proper local vector field, on open, simply connected sets that do not contain any disclinations. Globally, however, it has to be thought of as a director field. To make \mathbf{k} a proper vector field one needs to define it on two covers of the (x,y) plane which are connected with each other in the following way: if the number of disclinations is even, then the sheets are connected on curves that join the disclinations; if the number of disclinations is odd, then the sheets are connected on curves that join an even number of disclinations with the extra point joined to ∞ . This is analogous to the definition of $z^{1/2}$ as an analytic function on the double cover of the complex plane.

The director field nature of \mathbf{k} , although making global computation of θ impossible, is really not that bad. Director fields have topological signatures which can be used to locate defects. For example, let us look at the winding of the director field around defects. We have already noted that when you follow the director field continuously around a disclination it rotates through an angle of $\pm\pi$. In fact, around V (a concave disclination) the director twists through an angle of $-\pi$, while around an X (convex disclination) it twists by π . This twist is additive in the sense that, if there are several defects inside your contour, then the total twist of the director field is the sum of the twists of the individual defects. What is more, all point defects can be represented as composites of V and X. In Figs. 18(c) and 18(f) we have drawn a saddle (VV), a target (XX), a vortex (also XX), and a dislocation (XXVV). Because of the additive nature of twist, these composites have twists of -2π , 2π , 2π , and 0 , respectively, making their local \mathbf{k} into vector fields, and therefore they can be thought of as vector field singularities. In this case, we can define another topological quantity, the circulation, $\Gamma = \int_C \mathbf{k} \cdot d\mathbf{x}$, which is equal to the difference in phase as you integrate around the point defect. For example, $\Gamma(\text{dislocation}) = \pm 2\pi$.

There are other macroscopic order parameters which are useful in the characterization of patterns. We have already mentioned that, in order to reconstruct the microscopic dynamics from the wave-vector field, you need to know the local amplitude of the pattern (in the near-onset case this is simply $|W|$). At the onset of a new state, the amplitudes of the various modes play an important role in the initial competition for the dominant planform, as we have already seen in Secs. IV and IV.A. Far from onset, however, when the pattern has settled into some sort of equilibrium or quasiequilibrium state, the role of the amplitude is less important because it is slaved (algebraically related) to the wave vector almost everywhere. This is analogous to the situation with nonlinear oscillators, whose amplitudes and frequencies are algebraically related.

At some points in the pattern, notably at AGBs and dislocations, the amplitude is forced to zero, a fact compatible and consistent with the 2π circulation of a dislocation. Near such points, the amplitude is no longer slaved and has a dynamics of its own. Because of this, the neighborhood of points where the amplitude of the

pattern vanishes are ripe regions for the nucleation of new states. For example, it is often observed that when a roll pattern destabilizes to a hexagonal one, the hexagons will nucleate at dislocations in the roll field and vice versa.

Other macroscopic order parameters may also play a role in the pattern far from onset, but they tend to be more subtle and far less visible on the pattern photograph. Generally these correspond to the aforementioned soft modes of the pattern. Despite the difficulty in detecting these modes in the actual pattern, they play a central role in the pattern dynamics. In the context of the fluid problem, the soft mode is manifested as a large-scale horizontal mean flow, which is driven by large-scale pattern nonuniformities. Although one cannot see this flow in the pattern photograph, one can certainly see the effects. As we have noted, the presence of the mean flow serves to advect the phase contours so that sharp shapes, like the PGBs in Figs. 3–5, change to the more rounded, targetlike shapes of Figs. 6 and 7.

There are other possible reasons for curved textures in patterns (Cross and Meiron, 1995). If the microscopic system is a gradient flow, the dominant wavelength is $k = k_B$, which is the wave number where straight rolls are marginally stable to bending, and which is also the unique wave number preferred by circular patterns. In a gradient system, another important wave number, k_d , the wave number for which dislocations are stationary, is equal to k_B . However, if the microscopic system is non-gradient, k_d is in general different from k_B , and thus stationary patterns which contain dislocations will have roll patches where the wave number is $k_d \neq k_B$ (otherwise the dislocations would move, and the pattern would not be stationary). In such regions, one might well expect the constant phase contours to be more curved. There is also the possibility, in such cases, of “frustration” between k_d and k_B because of the competition between the two preferred wave numbers, which can lead to a continued time dependence of the pattern.

Far from onset, one does not have the advantage of a small-amplitude parameter. Nevertheless, the observation that the pattern consists of large patches of some planform (here we consider the roll case) in which the local wave vector changes slowly, suggests that we may be able to exploit another small parameter, namely, the inverse aspect ratio $\epsilon = \lambda/l$, where λ is the pattern wavelength and l is typically either the container diameter or the average distance between defects. We also know that there exist, in an infinite geometry, exact, 2π -periodic solutions,

$$w_0 = f(\theta; R, A) = \sum A_n \cos(n\theta), \quad (9)$$

to the microscopic equations. These correspond to the rolls that emerged at the first instability. So we ask: Do there exist slowly modulated solutions that can be represented as

$$w = f\left(\theta = \int \mathbf{k} \cdot d\mathbf{x}; A, R\right) + \epsilon w_1 + \dots, \quad (10)$$

where now $\nabla\theta = \mathbf{k}(\mathbf{X} = \epsilon\mathbf{x}, T = \epsilon^2 t)$ changes slowly in space and time? The correction terms w_1 , etc. are included in Eq. (10) because $f(\theta)$ is no longer an exact solution of Eq. (2). The correction term w_1 obeys a non-homogeneous linear differential equation obtained by linearizing Eq. (2) around $w = f(\theta)$ and having as a source the terms coming from the slow temporal and spatial variation of $\mathbf{k} = \nabla\theta$. However, if $f(\theta)$ is a solution of Eq. (2), so is $f(\theta + \theta_0)$, for any constant θ_0 , since this addition of phase simply represents moving the pattern in a direction normal to the wave vector. Thus $\partial f / \partial \theta$ solves the homogeneous equation for w_1 , which demonstrates that the linear operator acting on w_1 has a non-trivial nullspace, and consequently the forcing term must satisfy a solvability condition (the Fredholm alternative) in order for w_1 to exist. This solvability condition relates the spatial and temporal derivatives of θ and is called the phase diffusion equation. To order ϵ^4 it reads (with $\Theta = \epsilon\theta$, so that $\mathbf{k} = \nabla_x \theta = \nabla_X \Theta$)

$$\tau(k) \frac{\partial \Theta}{\partial T} + \nabla \cdot \mathbf{k} B(k) + \epsilon^2 \eta \nabla^4 \Theta = 0, \quad (11)$$

where τ can be thought of as a nearly constant, positive function of k , and η is a positive constant. For a broad class of problems, $B(k)$ has the roughly cubic profile seen in Fig. 19, although if the microscopic system is nongradient, then B is not analytic at its interior zero. The inclusion of the higher-order corrections to regulate Eq. (11) is necessary because, for certain values of k , $\nabla \cdot \mathbf{k} B$ is hyperbolic when written as a quasilinear, second-order operator in spatial derivatives acting on Θ . Consequently Eq. (11) is ill posed. This particular choice of regularization can be derived directly rather than inserted phenomenologically for a wide class of microscopic gradient flows.

To see that $\nabla \cdot \mathbf{k} B$ is hyperbolic, set $\epsilon = 0$ in Eq. (11) and linearize about the roll solution by setting $\Theta = \mathbf{k} \cdot \mathbf{X} + \psi$ to find

$$\tau(k) \psi_T + B \psi_{YY} + \frac{\partial}{\partial k} (k B) \psi_{XX} = 0. \quad (12)$$

Thus the signs of $k B$ and $(k B)_k$ determine the stability of rolls. For narrow rolls with wavelengths shorter than $2\pi/k_E$ (see Fig. 19), $(k B)_k$ is positive and the rolls are unstable to perturbations in the direction of their wave vector. This instability corresponds to the aforementioned Eckhaus instability. For rolls that are fatter than $2\pi/k_B$, $k B$ is positive and the rolls are unstable to the zigzag instability, which results in an interaction between the modes $(k, 0)$ and $(k, \pm \sqrt{k_B^2 - k^2})$. This instability is saturated by the presence of the regularization and nonlinear terms and leads to the phase grain boundary solution,

$$\Theta = k_B X \sin(\alpha) + \ln\{2 \cosh[k_B Y \cos(\alpha)]\} \quad (13)$$

with bend angle 2α ($\alpha = \pi/2$ corresponds to straight rolls). The region $k_B \leq k < k_E$ for which $\nabla \cdot \mathbf{k} B$ is elliptic negative is called the Busse balloon (Busse, 1978) and

corresponds to a band in which straight rolls with wavelength $2\pi/k$ are linearly stable.

And now a miracle occurs. We observe that Eq. (11) can be written as a gradient flow

$$\frac{\partial \Theta}{\partial T} = - \frac{\delta F}{\delta \Theta} \tag{14}$$

with free energy

$$F[\Theta] = \int \frac{1}{2} \epsilon^2 (\nabla^2 \Theta)^2 + \frac{1}{2} G^2(k) dx, \tag{15}$$

$$G^2(k) = - \frac{1}{\eta} \int_{k_B^2}^{k^2} B(k) dk^2, \tag{16}$$

with two contributions. The first is the cost of roll bending, while the second is the cost of the wave number's being different from the optimal k_B . An infinite field of rolls with $k=k_B$ of course minimizes F , but because of the constraints of boundary conditions, etc., this is not viable for us. We expect the minimizing solutions to be ones which almost everywhere have $k=k_B$, but where the bending contributions come into play on point and line defects.

A little calculation will show that, for the solution given in Eq. (13), the two terms of the energy balance exactly. There is no *a priori* reason we should have expected this. Encouraged to exploit this fact, we may ask: When do solutions of

$$\epsilon \nabla^2 \Theta = \pm G \tag{17}$$

satisfy the time-independent version of Eq. (11), i.e., minimize $F[\Theta]$ from Eq. (15)? The answer is whenever $J = f_X g_Y - f_Y g_X$ [where $\mathbf{k} = (f, g)$], the Jacobian of the map from \mathbf{X} to \mathbf{k} is zero (Newell *et al.*, 1996). The quantity J is proportional to the Gaussian curvature of the phase surface Θ and is exactly zero for the knee solution in Eq. (13).

Not only is Eq. (17) a reduction of the original phase diffusion equation, but, to a good approximation, it can also be linearized. The reason is that $G \approx |k^2 - k_B^2|$ so that Eq. (17) is just

$$\epsilon \nabla^2 \Theta = \pm [(\nabla \Theta)^2 - k_B^2], \tag{18}$$

which linearizes to the Helmholtz equation,

$$\epsilon^2 \nabla^2 \psi - k_B^2 \psi = 0, \tag{19}$$

via the transformation $\Theta = \pm \epsilon \ln \psi$. Now, for rather general cases, we can show that the asymptotic ($\epsilon \rightarrow 0$) solutions of the phase diffusion equation have the property that $J=0$ almost everywhere. The story does not end here, however.

Because J is proportional to the Gaussian curvature of the phase surface, we can bring to bear a variation of the Gauss-Bonnet theorem, relating curvature and twist. A little analysis (vector calculus and the divergence theorem) shows that

$$2 \int_{\Omega} J dx dy = \int_{\partial \Omega} k^2 d\phi. \tag{20}$$

But, if $k=k_B$ on the boundary $\partial \Omega$ of Ω , the right-hand side of the above equation simply measures the twist discussed in Sec. V. Because this twist is a topological quantity, J must be conserved on regions with $k=k_B$ on their boundaries. Furthermore, because of energy considerations, we can expect to see $k=k_B$ across large regions of the pattern, and, consequently, $J=0$ except at point defects, the centers of twist, and perhaps on some line defects. The reader can see that as $\epsilon \rightarrow 0$ the curvature term in F becomes less important and $k \rightarrow k_B$ across the pattern. Thus, in the small- ϵ limit, J must focus in on points like a δ function, although with possibly non-trivial angular dependence, or on PGBs joining point defects. Thus the graph of the phase surface θ , as drawn on a double cover of the (x, y) plane, resembles a piece of crumpled paper with many flat surfaces and all of the Gaussian curvature stored in point defects. The reason for the focusing behavior of the Jacobian (Gaussian curvature), as well as the nature of the singularities of J , remains an open problem.

VI. WAVELETS—A BRIDGE BETWEEN THEORY AND EXPERIMENT

At this point the reader should appreciate the general dichotomy inherent in the study of patterns. Experimentalists, both physical and computational, produce patterns in the microscopic field variables. Most of the theoretical work on patterns, however, relies on the knowledge of macroscopic order parameters, like the local wave-vector field \mathbf{k} . It would be desirable to have a way of transforming one to the other. We have already mentioned ways of reconstructing the microscopic signal (at least locally) from the order parameters. What remains is a way of extracting order parameters from real signals.

To this end we want to find a way to transform the microscopic field into the order parameters. This transformation should be local in space, to account for the slow variation of the order parameters, a criterion which eliminates the usefulness of the ordinary Fourier transform because, while it is local in wave number, it is completely nonlocal in space. The power spectrum one would obtain from Fourier-analyzing the pattern would give information on the average rather than the local wave vector. Despite this difficulty, Fourier methods are often used in pattern analysis to attempt such order-parameter extraction, but they are not perfect. Instead let us look for a local version of the Fourier transform. Several such objects exist and have been well studied, and, of all of them, the continuous wavelet transform seems to best suit the goal of extracting order parameters.

The continuous wavelet transform is much like the Fourier transform, except that instead of convoluting the pattern with dilated and rotated plane waves $e^{i\mathbf{k}\cdot\mathbf{x}}$ one uses dilated, rotated, and translated copies of a wave packet (say a Gaussian amplitude over the carrier wave). The transform is now local in both space and wave number, at the cost of introducing an extra degree of freedom, the location of the center of the wave packet.

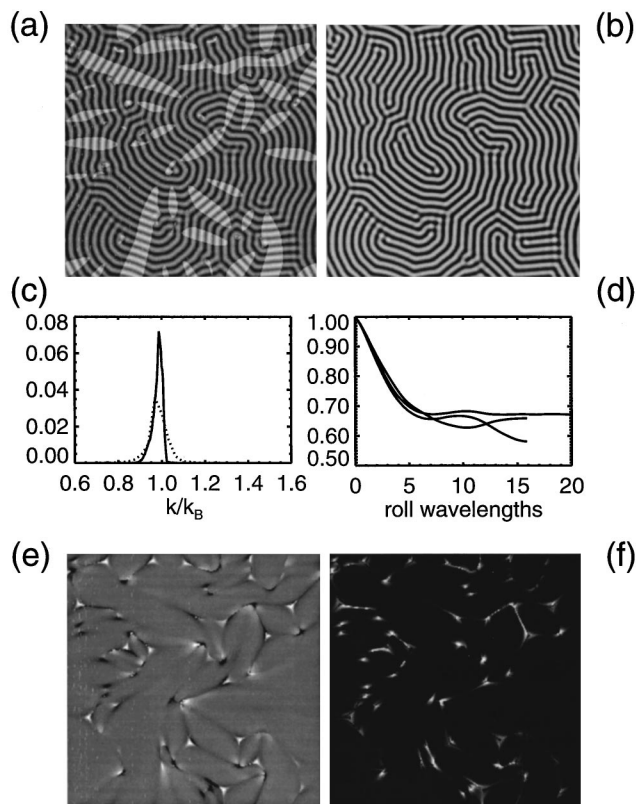


FIG. 20. Numerically generated pattern after wavelet analysis: (a) the pattern with regions of high $k > k_B$ marked in white; (b) the pattern itself; (c) the wave-number histogram computed with the wavelet algorithm (solid line) as well as with Fourier transform techniques [the structure function averaged over angle (dotted line)]; (d) the correlation of the pattern along various cross sections (horizontal, vertical, and diagonal); (e) the Jacobian of the map; (f) the magnitude of L , the curl of the vector field \mathbf{k} .

The basic idea behind the wavelet analysis of a pattern is simple and takes advantage of the fact that the order parameters of the pattern vary slowly with respect to the pattern wavelength λ . To determine the local wave number at a particular spot in the pattern, simply lay the wave packet you choose over the pattern, centered on the point of interest. Now dilate and rotate the wavelet until its wave vector matches the local wave vector of the pattern. Do this at every point in the pattern, and you extract the local wave vector everywhere in the pattern. Once this is available, other order parameters like amplitude and mean flow are easily reconstructed, both at points where they are slaved and at points where they are not. For more detail we refer the reader to Tchamitchian and Torr sani (1992), Guillemin and Kronland-Martinet (1996), and Bowman *et al.* (1997). Readers are also invited to investigate more general works on wavelets, for example, Daubechies (1991), Farge (1992), and Meyer (1993).

Wavelet analysis gives exactly what is needed to make the connection between experiment and theory, namely, the order parameters. With the wave-vector field known, it is easy to compute important derived quantities of the

pattern, like the phase diffusion energy density F , or J , the Jacobian of the map from \mathbf{X} to \mathbf{k} . Knowledge of J , and where it gets large, provides a convenient way to detect and locate point defects. Once the location of these points are known, the wave-vector field can be used to compute topological quantities like twist and circulation in order to classify the types of defects. An example of this analysis and the kind of information it allows you to extract is shown in Fig. 20.

The wavelet transform allows one to extract wave vector information from the pattern. Consequently it is easy to compute pattern wave number histograms, as shown in Fig. 20(c). This analysis can also be performed with Fourier methods, but the nonlocality of the transform makes it inherently less accurate and tends to broaden the resulting histogram by a large amount. An accurate histogram allows one to make important statements about the pattern, such as whether the pattern lies in the stable region of the Busse balloon, for example. Furthermore, since the wavelet transform is local, the histogram data can be viewed spatially, showing at a glance where the pattern has wave number greater than k_B , for example [Fig. 20(a)]. Since the wave-number data extracted from the wavelet algorithm are smooth, it is easy to compute quantities like J [Fig. 20(e)] or the curl of the wave vector \mathbf{k} [Fig. 20(f)]. Finally, the possibility exists that the wavelet-based algorithm outlined in Bowman *et al.* (1997) can be conveniently implemented optically. If this is the case, it may be possible to build a device that would implement this algorithm “on the fly” and provide experimentalists a real-time look at the order parameters in their systems.

Other methods that do not involve the wavelet transform have been recently proposed. In particular Egolf *et al.* (1998) use derivatives of the pattern intensity to extract \mathbf{k} . Their method appears to be very computationally efficient, and shows promise for the future.

VII. CONCLUSION

Patterns are macroscopic objects whose behaviors are governed by universal equations. The structure of these equations depends on the overall symmetry properties of the original system, rather than on its microscopic details. While progress on the computational, experimental, and theoretical fronts has been encouraging, there are many, many open problems. We invite you to come explore this wonderful world with us.

REFERENCES

- Assenheimer, M., and V. Steinberg, 1994, *Nature* (London) **367**, 345.
- Assenheimer, M., and V. Steinberg, 1996, *Phys. Rev. Lett.* **76**, 756.
- B nard, H., 1990, *Ann. Chim. Phys.* **7** (Ser. 23), 62.
- Bowman, C., T. Passot, M. Assenheimer, and A. C. Newell, 1997, *Physica D* (in press).

- Busse, F. H., 1978, Rep. Prog. Phys. **41**, 1929.
- Cross, M. C., and P. C. Hohenberg, 1993, Rev. Mod. Phys. **65**, 851.
- Cross, M. C., and D. Meiron, 1995, Phys. Rev. Lett. **75**, 2152.
- Daubechies, I., 1991, *Ten lectures on Wavelets*, CBMS Lecture Notes Series (Society for Industrial and Applied Mathematics, Philadelphia, PA).
- Edwards, W. S., and S. Fauve, 1994, J. Fluid Mech. **278**, 123.
- Egolf, D. A., V. I. Melnikov, and E. Bodenschatz, 1998, Phys. Rev. Lett. (to be published).
- Farge, M., 1992, Annu. Rev. Fluid Mech. **24**, 395.
- Gollub, J. P., and H. L. Swinney, 1975, Phys. Rev. Lett. **35**, 927.
- Guillemain, Ph., and R. Kronland-Martinet, 1996, Proc. IEEE **84**, 561.
- Joets, A., and R. Ribotta, 1986, J. Phys. (Paris) **47**, 595.
- Joseph, D. D., 1976, *Stability of Fluid Motions Vol. I and II* (Springer, Berlin).
- Kolodner, P., C. M. Surko, and H. Williams, 1989, Physica D **37**, 319.
- Kondu, S., and R. Asai, 1995, Nature (London) **376**, 765.
- Koschmieder, E. L., 1974, Adv. Chem. Phys. **26**, 177.
- Lega, J., J. V. Moloney, and A. C. Newell, 1995, Physica D **83**, 478.
- Meyer, Y., 1993, *Wavelets: Algorithms and Applications*, translation by R. D. Ryan (Society for Industrial and Applied Mathematics, Philadelphia, PA).
- Murray, J. D., 1989, *Mathematical Biology* (Springer, Berlin).
- Newell, A. C., T. Passot, C. Bowman, N. Ercolani, and R. Indik, 1996, Physica D **97**, 185.
- Newell, A. C., T. Passot, and J. Lega, 1993, Annu. Rev. Fluid Mech. **25**, 399.
- Pesch, W., 1996, Chaos **6**, 348.
- Rayleigh, Lord, 1916, Proc. R. Soc. London, Ser. A **93**, 148.
- Seul, M., L. R. Monar, L. O. Gorman, and R. Wolfe, 1991, Science **254**, 1616.
- Surko, C. M., 1993, private communications.
- Swift, J. B., and P. C. Hohenberg, 1977, Phys. Rev. A **15**, 319.
- Tchamitchian, Ph., and B. Torrèsani, 1992, in *Wavelets and Applications*, edited by M. B. Ruskai *et al.* (Jones & Bartlett, Boston), p 123.
- Thompson, D., 1942, *On Growth and Form* (Cambridge University, London).